DETONATION WAVES IN GASES

A. A. Vasil'ev, V. V. Mitrofanov,
and M. E. Topchiyan

Gas detonation has attracted increased interest in the last decade because of technological problems, explosion hazards in mining, and other problems in technology and power engineering, including nuclear. Although on the whole the one-dimensional theory describes detonation-wave (DW) behavior quite satisfactorily, detailed studies have shown that the front structure is always cellular (see bibliography in [1]).

Most current studies envisage these structures and transverse waves. The cell size is a characteristic dimension used to scale the phenomena: reaction-zone sizes, detonation-tube and free-charge diameters, channel dimensions, roughness and obstacle sizes, initiation energy-distribution zones, turbulent-pulsation scales, etc.

A single journal paper cannot deal with all the problems and papers on gas detonation and explosion. On the other hand, it is necessary to survey the physical results obtained recently. Without striving for completeness, we consider mainly lines that have involved the Siberian gas-detonation school, whose first researches were directly related to the founding of the Siberian Division, Academy of Sciences of the USSR, 30 years ago.

1. AVERAGE MULTIFRONT DETONATION PARAMETERS

Since the one-dimensional DW model was completed in [2], tests have been made on it, the most important parameters being: the detonation rate D, the extent, the maximum chemical peak pressure p_{cp}, and the pressure p_c and the density ρ_c at the Chapman–Jouguet point. Various methods [3-6] have invariably given pressures and densities at the chemical peak and the Jouguet point lower than those from the one-dimensional theory, although the point position is determined rather arbitrarily. The observed detonation speeds $\overline{D}$ as a rule are somewhat lower than the calculated D_0, although elevated values have sometimes been observed. The velocity deviation $\Delta D = D_0 - \overline{D}$ and the dependence on tube diameter d (linear relation between ΔD and $1/d$) can be explained to a first approximation by wall loss. Pressure underestimation is due mainly to the inadequate spatial and time resolution.

Complex inhomogeneous wave structures have given the problem a new meaning. One now has to consider the correspondence between the average wave parameters and the one-dimensional theory, although it is often far from simple to interpret the measurements.

Pressure. The pressures have been measured [7, 8] with piezoelectric sensors having sensing surfaces of size representing a considerable part of the expected chemical peak size. The maximum pressures at that peak are less than those predicted by the one-dimensional theory, and a fit can be obtained only by extrapolating the data.

Improved resolving power gives hope for more accurate results. In [9], the average p profiles were constructed from a large number of waveforms recorded with a circular sensor whose size was less than the cell size by about a factor 20. The waveforms gave a relation between p_{cp} and p_c. The maximal p_{cp} in multifront detonation was 10-20% less than the theoretical one-dimensional value. The same study demonstrated a triangular profile on average for the chemical peak.

In [10], systematic measurements were made on the pressures in the forward and reflected waves by means of sensors whose resolving power was reduced to 0.1 μsec for measurements in the forward wave or 0.05 μsec for the wave reflected from the ends. At low initial pressures p_0, the results for the two waves agreed well with the one-dimensional theory, but as p_0 increased, there were increasing deviations, with the measured values becoming less and the resolving power becoming inadequate.

Novosibirsk. Translated from Fizika Goreniya i Vzryva, Vol. 23, No. 5, pp. 109-131, September-October, 1987.

0010-5082/87/2305-0605$12.50

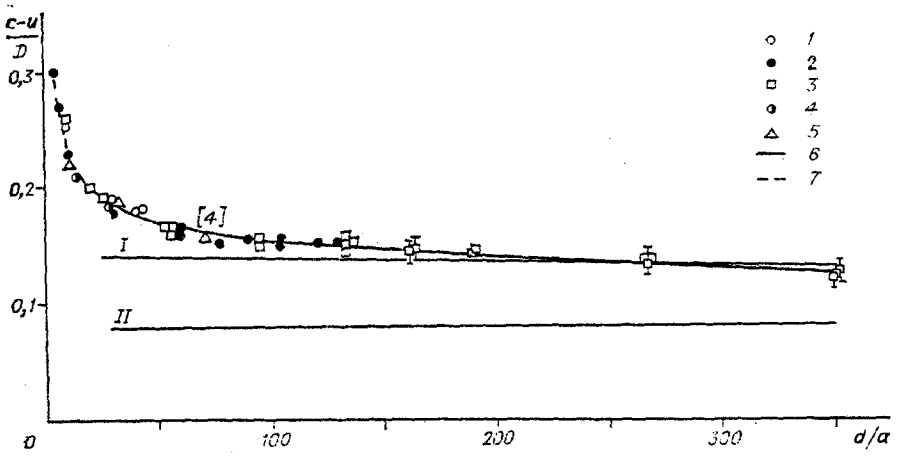

Fig. 1. Speed of a weak perturbation behind a detonation front: I and II) frozen and equilibrium values of (c − u)/D correspondingly; 1) $2H_2 + O_2$; 2) $2H_2 + O_2 + 3Ar$; 3) $C_2H_2 + 2.5O_2$; 4) $C_2H_2 + 2.5O_2 + 10.5Ar$; 5) $CH_4 + O_2$; 6, 7) d = 80 and 21 mm.

Pressure interpretations require some caution, since pulsations may increase the measured pressure above the static mean [11]. Averaging the pressure along the front for different pulsation phases should [12] reduce the mean value by comparison with a smooth wave. Velocity pulsations may explain the differences between [9] and [10] on the chemical peak, since one of the pulsating velocity components was absent in [9], as measurements were made in channel where one dimension was less than the cell size (the flow was virtually planar).

Chapman–Jouguet Surface. A constant mean detonation speed indicates that a multifront wave has a physical analog of the Chapman–Jouguet plane, namely a flow surface or region where there is a transition from subsonic flow in the front system to supersonic. Measurements have been made [13, 14] to locate this surface. The studies involved DW in a tube having a cellophane wall. It was assumed that the distance of the Chapman–Jouguet surface from the front was not less than the cross section at which the flow expanded because the tube wall failed and thus led to a reduction in the wave velocity exceeding the error of measurement. Measurements were also made on the instant of detachment for the shock wave arising when it reached a thin knife edge, which corresponded to the gas speed u in the laboratory frame of reference passing through the speed of sound c. In a planar wave, the u = c section represents a point limiting the approach of the Chapman–Jouguet surface to the front. This surface in a multifront wave extends to distances from the front corresponding to several cell diameters.

Quantitative checks have been made on the Chapman–Jouguet condition (selection rule) by measuring the perturbation speed c − u for upstream motion. It has been found [15] that c − u deviated from the calculated value. Exact calculations [16] showed that $\psi = (c - u)/D$ is very sensitive to deviations from the Chapman–Jouguet state. Measurements (Fig. 1) revealed a single dependence of ψ on d/a (a is cell size) for different mixtures and tube diameters. For d/a small, ψ corresponds to states on the detonation adiabat lying below the Jouguet point, while as d/a increases, ψ approaches the value corresponding to the Jouguet condition for the frozen speed of sound [16].

Several attempts have been made to formulate the selection rule with allowance for inhomogeneities and pulsations within the one-dimensional theory; the first examples employed homogeneous isotropic turbulence [17-19]. Introducing special formal variables enables one [11] to reduce the treatment for a turbulent flow to one for a smooth wave.

In [20, 21], the selection rule was constructed for any equation of state and any dependence of the square of the pulsation velocity ε on p and ρ. In the particular case γ = const and a power-law dependence of ε on ρ, formulas were obtained for the deviations in wave speed and Chapman–Jouguet point parameters for the classical model. These formulas show that the observed deviations can be explained by turbulent pulsations.

2. EQUILIBRIUM CALCULATIONS ON DETONATION PARAMETERS AND KINETIC SIMULATION

Steady-state DW measurements are usually compared with equilibrium-flow calculations for chemically reacting gases. The first papers appeared in the early 1960s [22] giving detailed information on Chapman–Jouguet states for mixtures of hydrocarbons with oxygen and air. Extensive calculations have been given [20, 23] for mixtures containing C, H, O, and N in the gaseous state and for various initial compositions not excessively enriched in carbon atoms. The results relate not only to Chapman–Jouguet states but also to shock and equilibrium detonation adiabats (overcompressed and undercompressed branches) as well as closed-volume combustion parameters and direct reflection. The equilibrium adiabats are similar for a wide velocity range, which gave simple approximate formulas for the basic gas-dynamic parameters for various initial conditions. Exact values were obtained for the reduced heat of reaction on overcompression. As the wave speed increased by not more than a factor two in any gas mixture, the reaction heat passed through zero. Heat removal also provided effective damping because the equilibrium was shifted.

In [24] there are equilibrium calculations for other mixtures, including ones containing free carbon in the products. In [25], the methods of [23] were used to analyze ternary configurations involving spin detonation. In [26], equilibrium flows were calculated for cryogenic initial conditions with a van der Waals equation of state for hydrogen–oxygen mixtures.

The kinetic equations are cumbersome, which complicates flow analysis and makes it impossible to employ an analytic approach. The dissociation energies are approximately equal to the diatomic and triatomic molecules usually present in detonation products, so a simple kinetic model is possible, where a single differential equation describes the energy production and the molecular-mass change [27]. It is mentioned in [28] that such a description is possible, but in [27] the model was carried through to analytic formulas.

3. WALL EFFECTS AND DETONATION LIMITS

Detonation in Wide Tubes. The kinetic model [27] has been used in a detonation model for wide tubes, which incorporates loss [29]. Tube diameter increase does not lead to asymptotic transition to a state corresponding to lossless detonation. The relative loss level persists as d increases, while the distance from the front to the Chapman–Jouguet surface increases. This is confirmed qualitatively by measurements [13, 14] on ψ (Fig. 1) and the Chapman–Jouguet surface (see above), but it does not agree with the results of [30, 31], where it was found that the supersonic region indicated by stationary Mach lines for $d/a \gg 1$ is at a distance of several cell diameters from the front. One clearly needs a more careful analysis of the chemical factors, turbulence damping, energy and momentum loss at the wall, and boundary-layer effects.

These factors are also decisive for another area: detonation limits.

Near-Limiting States. The limit mechanism is qualitatively clear [2, 32]: reaction-zone enlargement leads to heat and momentum loss from the region between the shock wave (SW) and the Chapman–Jouguet surface, which reduces the wave speed and causes additional reaction-zone expansion, etc. A critical situation arises, where self-maintaining wave propagation becomes impossible.

Spin detonation with a unique transverse wave (TW) has been examined in detail for circular tubes, where the wave moves in a spiral along the wall [18]. That state arises in a tube having $d \approx (0.5\text{-}0.3)a$ [33, 34]. In a rectangular channel, it corresponds to a DW having one or more transverse waves, which move along the larger side. Quasispin also occurs in a square tube [35]. It has been shown [36] that the state with a unique transverse wave can occur in a rectangular channel only if the ratio of the larger and smaller sides is $H/h \leq 2$, while if $H/h > 2$, the limiting state is one with several transverse waves.

Interest attaches to the spin diameter for a stoichiometric methane–air mixture, which is the most difficult to detonate. It has been reported [37] that the detonation could be excited in a 60 mm tube, but the result was not subsequently confirmed [34]. We have found that stationary spin detonation with a single transverse wave can occur at $p_0 = 1$ atm in a tube having $d = 100$ mm, where the spiral pitch (the analog of the cell size) was about 31 cm.

Below the spin-detonation limit, a circular tube can show a nonstationary self-maintained (so-called galloping) detonation state [38, 39], which occurs for $d < a/\pi$ and has periodic longitudinal pulsations having a step of the order of hundreds of times the diameter, with repeating detonation halts and reinitiation. After reinitiation, an overcompressed multifront wave is excited, and the front structure enlarges as this weakens, with passage through a spin-detonation stage, which then is damped out, and the SW is detached from the flame front. After a time, a flare-up occurs near the flame front and a DW forms rapidly, which accelerates up to the shock front. Then the process repeats. This state expands the limits for self-maintaining wave propagation beyond the spin-detonation region in mixtures giving irregular cellular structures. A closed model has been proposed for galloping detonation [39], which describes the main characteristics.

Free-Charge Detonation. One has to determine critical detonation diameters for free explosive cylinders in various aspects of explosion physics, particularly explosion safety. It has been shown [40, 41] that a detonation can propagate in the free gas column obtained by retention in a stretched rubber tube, which indicated that all previous experiments with weak walls had underestimated the critical diameter. Improvements in the method [42] enabled one to detonate a jet of explosive gas embedded in an air flow. The diffuseness at the boundary between the explosive gas and the air was much reduced, and the length of the free gas column attained 20-25 times the diameter. Stoichiometric and equimolar acetylene–oxygen mixtures were used to show that the ratio of the critical diameter to the cell size as measured for detonations under these conditions in a strong tube is about 60, where it was found that DW propagation in $2H_2 + O_2$ ($a = 1.5$ mm) cannot occur in a layer of thickness 35 mm above a solid surface, which is in contrast to calculations [43, 44]. A layer of a propane–butane mixture with oxygen of thickness up to 20 mm ($a \approx 1$ mm) would not give stationary detonation [42]. The relation $d_*^c/a \approx 60$ can be used to estimate the sizes of free gas charges in other gas mixtures.

Channels Containing Obstacles: Porous Media. If the tube is free from roughness and $d \approx 1$ cm or more, the wave speed at the detonation-propagation limit is reduced by not more than 10-15% on account of wall loss [2].

If the roughness is considerable, the detonation-speed range extends considerably down to about $0.5D_0$ or less [45, 46]. In many industrial gas and gas-dust explosions, such as methane in mines, the velocities are highly nonideal (about 1 km/sec), and the extended shock-compressed gas plug at the head of the wave may mean that the destructive effects are no less than those in ideal detonation [47].

Artificial periodic obstacles have been used as contractions in a flat channel [48, 49] or ring inserts and Shchelkin spirals in tubes [47, 50-52], which have shown that there are two states of supersonic explosion-wave propagation: high speeds ($\bar{D} \geq 1000$ m/sec) and low speeds ($\bar{D} \approx 500$-800 m/sec, sometimes less), with a step transition between them (dashed line in Fig. 2).

In the high-speed state, the ignition is provided by an SW in the forward direction reflected from the obstacles, where there are periodic interruptions in the shock-wave ignition, which is replaced by convective flame transport and then reverse transition to shock-wave ignition. In the low-speed state, the shock-wave mechanism is eliminated completely, and the ignition is transferred convectively by hot product jets. The state is dependent on the channel parameters and the mixture composition and pressure. There is a narrow initial-pressure range in which the state is dependent on the initiation conditions [49]. The low-speed state also exists [53] in narrow channels without artificial obstacles, but the mechanism requires additional research. The low-speed state has been called [48, 49] the low-speed gas-detonation state or [47, 52] explosive combustion. It has detonation features (supersonic velocity, pressure and density increase at the front) as well as ordinary convective-burning ones (as regards propagation mechanism), and it is an intermediate state not envisaged in the classification.

The high-speed state goes over continuously to the low-speed one on gas-mixture detonation in inert porous media (sand, gravel, metal filings, balls, etc.) if the pressure is reduced as shown by the solid lines in Fig. 2 (various mixtures and pore sizes). The measurements have been made for particle size of 30 μm to 12 mm and pressures of 10^4-10^7 Pa [48, 54-57]. There is no sharp boundary between the states because the pores vary in shape and size, and the ignition mechanisms alter at different times in these. Stationary subsonic burning waves can exist only in not very active mixtures such as fuel–air ones

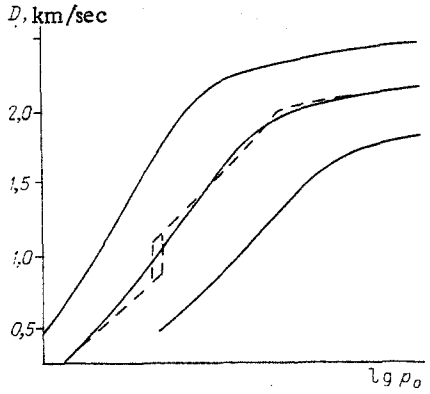

Fig. 2. Gas detonation speeds in channels of periodically varying cross section (dashed line) and in porous media.

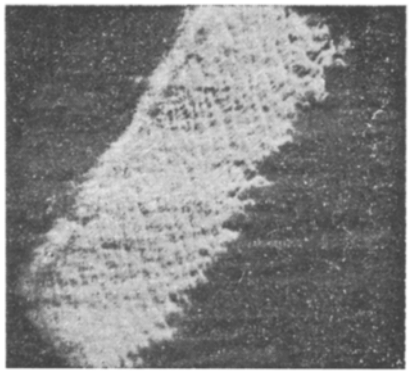

Fig. 3. Trace imprint of transverse-wave fine structure.

below the lower limit for low-speed detonation (as regards pressure, concentration, or particle size). Slow burning of a stoichiometric fuel–oxygen mixture in such a medium is unstable and goes over rapidly to detonation.

The lower bound to the low-speed state in certain cases is displaced below the speed of sound in a profiled channel [49] and in a porous medium [57], which shows that SW are unimportant in that state.

4. CELLULAR STRUCTURE

Soon after the phenomenon of cellular multifront detonation was discovered, detailed studies were made on it [18, 58]. Subsequent research has been concerned, on the one hand, with defining the effects on the characteristic cell size and on the other with detailed research on the structure to provide information on the phenomenon. Cellular structures occur at initial pressures up to 10 atm [59], while the improved resolving power from the trace method enables one to detect cells of characteristic scale down to 0.02 mm. Such small cells are formed in particular in transverse spin-detonation waves in methane–oxygen mixtures (Fig. 3 [60]).

The transverse cell size a usually has a power-law relationship to the pressure [18, 58-63], i.e., $a = a_0(p_0/p)^s$, where a_0 and s are mixture constants ($s \approx 1$). A U-shaped curve having its minimum between the stoichiometric and equimolar compositions applies for any given fuel for the relation between cell size and fuel-oxidant ratio [34, 63, 64]. Measurements have been made on initial-temperature effects [65], and on the simultaneous effects of temperature and pressure [66], where cell-size measurements were made for DW propagating in a gas previously compressed and heated by an SW. It has been shown [62, 67] that small amounts of inhibitors affect multifront-wave characteristics.

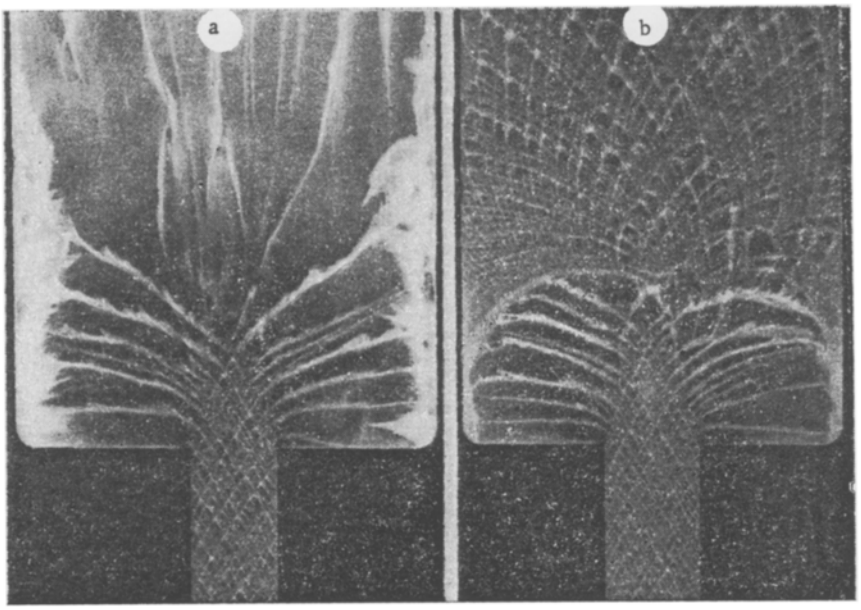

Fig. 4. DW emerging from a narrow channel into a wide one: a) DW damping; b) detonation reinitiation.

The structure scale increases [68-75] on wave attenuation by flow around a convex surface or a corner, on emergence from a narrow channel into a wide one (Fig. 4), and on going from one mixture to another. The cell size is reduced on compression. In [76], an overcompressed wave occurred on transition from a large-diameter tube to a small-diameter one via conical junction, while in [77], the cell structure was examined for a Mach detonation front arising on irregular reflection at a wedge.

Stability and the relation between energy release and wave speed are aspects closely related to the speed dependence of the cell size. In [78] it was shown that an initially smooth front in a highly overcompressed wave gives rise to small-scale inhomogeneities at a certain stage in the attenuation, which occurs at speeds such that the transition from the state behind the SW to complete chemical equilibrium occurs without pressure change. The cells cease to be identified not because of inadequate resolution but because the front becomes smooth. It is not found that there is a correlation between the limit for the structure to occur and the E_a/RT parameter: the boundary is correlated with zero energy production. As the degree of overcompression decreases and the wave approaches the stationary state, the cells enlarge up to the mean size. There is similarity between mixtures in the overcompression dependence for the cell size [76, 77].

The evidence shows that cell structures in impressions differ in regularity, where there are three classes: regular, irregular, and intermediate (quasiregular). The first occurs in mixtures containing considerable amounts of argon. Irregular structures are typical of fuel–air mixtures, and intermediates ones of most fuel–oxygen ones. Although the boundaries between the states are fairly nominal, the extreme situations are prominent. Measurements and estimates [60, 78-80] show that E_a/RT is the parameter governing the regularity, where E_a is the activation energy for the main reaction in the induction period and T is the temperature in the induction zone behind the planar stationary wave moving with the detonation speed. Small E_a/RT correspond to more regular structures. The argon effect shows that the DW energy and γ can affect the regularity. Also, the regularity is related to DW stability, which is affected by the activation energy and the energy production [81]. It has been confirmed [82] that E_a/RT is basic to DW stability, where it was found that E_a/RT above 6.2 correspond to a fine structure (small cells) within the basic ones.

Mixtures with large-scale regular structures have provided relations between the kinematic parameters [18, 58, 67, 83-86]. In the time between two successive collisions $t_c = b/\overline{D}$, where b is the longitudinal cell size and $\overline{D}$ is the mean detonation speed, the leading front changes in velocity from $(1.8\text{-}1.4)\overline{D}$ at the start of the cell to $(0.6\text{-}0.85)\overline{D}$ at the end. The form of leading front in a regular cell is close to an arc of a circle, whose radius is about 1.3 times the distance from the cell start. Transverse waves also have

variable velocities. There are no such detailed data for irregular cells, since the events are to some extent chaotic, but here one still finds the main characteristic features of the nonstationary motion in ordered structures.

Measurements have been made [12, 87] on the contributions from structure elements during combustion; part of the mixture (not less than half) burns after single shock compression by the leading front, while the rest enters the transverse waves. Cases occur where the mixture does not burn completely even after double shock-wave passage (initially the leading SW and then the transverse one), and there are initial-mixture islands in the reaction zone, which burn up much later. It has proved possible to trace stages in transverse-wave collision, where an interesting but unexpected effect is that cumulative jets are formed [88]. The fronts in the various phases are nonstationary, so one gets a large variety of interaction forms [89].

The contributions from the elements alter with p_0 and composition, which implies lack of geometrical similarity [12, 87]. The changes are more pronounced at low p_0.

In spite of the obvious progress in the picture of multifront detonation, there are unsolved problems concerning transverse-wave multiplication at divergent cylindrical or spherical fronts, particularly stability loss and the production of new ignition foci [11].

Theoretical Cell Models. The first attempt [58] to relate the cell size to mixture properties was based on an idealized two-front DW model having an induction zone and instantaneous reaction, where the parameter was the induction zone length λ behind a planar stationary SW moving with speed D_0. There is direct proportionality between a and $\lambda = (D_0 - u)\tau$ only when the induction zone is much longer than the recombination (energy-release) one [61]. If the two are comparable, the relationship is much more complicated. The λ were calculated from a complete system of tested kinetic equations and were compared with the measured a in [90]. An approximately linear relation of the form $a = k\lambda$ was obtained, where k = 20-35.

In [91], a geometrical-acoustics model was used to consider perturbation simulating a transverse wave; the quantitative results from this model and subsequent forms of it remained inexact, although better agreement was obtained in the later studies [92]. A deficiency of the acoustic approach is that real shock-wave interactions are neglected.

In [87], the relation between cell size and mixture characteristics was derived from the condition for ignition halt behind an expanding cylindrical front having a decreasing speed. The empirical law for the speed D(r) was used with the additional assumption that the breakaway occurs at the point where $D = D_0$, which gave the longitudinal cell size:

$$b \simeq \frac{E_a}{RT} D_0 \xi \tau_0, \tag{1}$$

where τ_0 is the induction time behind the planar SW moving at a constant speed D_0, while $\xi \approx 1$ (it varies from about 0.5 to 2 in accordance with the adiabatic parameter and the choice of termination conditions [124]).

A closed model has been given [93] for a two-dimensional cell, which incorporates the actual processes and enables one to calculate all the main parameters without resort to experiment; this was supplemented in [76, 94]. In it, a gas detonation front propagates with periodic TW collisions (Fig. 5), each of which is equivalent to a local microexplosion, which generates a cylindrical DW, whose speed gradually falls below $\overline{D}$. At the initial stage, the ignition delays are very short, and the flame front adjoins the SW; as the wave weakens, the induction time increases catastrophically at $r = r_*^c$, and the flame becomes detached from the SW and almost ceases to be displaced. A layer of compressed unburned gas accumulates between the SW and the flame front, in which the TW collide and start a new cycle. Two stages represent the leading-wave motion: with instantaneous combustion as the wave propagates on the part up to r_*^c and with no energy supply after r_*^c. The speed is described via the TW collision energy and the heat production in the gas burning behind the leading wave, where one can employ interpolation formulas that in limiting cases give the wave speed for a strong point explosion or the Chapman–Jouguet speed. On the assumption that the induction period ends when the TW collide, the model provides formulas for the basic cell parameters, namely

$$b = \frac{2(\gamma_0 - 1)}{\gamma_0 - 1} \frac{D_* \sigma_*}{x_*} \frac{E_a}{RT_*} \tau_* \tag{2}$$

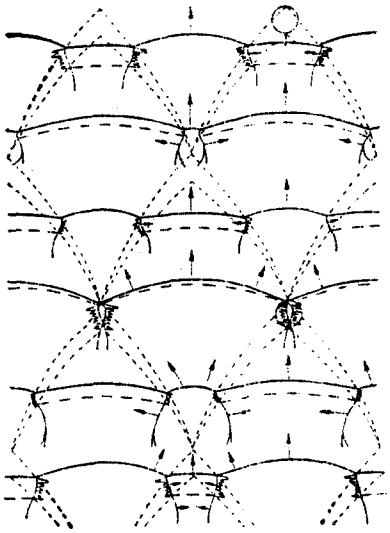

Fig. 5. Scheme for a two-dimensional DW cellular structure: solid line shock and detonation front; dashed line combustion fronts; close-dashed line traces of transverse waves; the circle shows transverse-wave collision.

and the detonation initiation energy for a cell

$$E_{02} \approx 0{,}22\,\rho_0 D_0^2 b^2, \tag{3}$$

where γ_0 and ρ_0 are the adiabatic parameter and density for the initial mixture, σ is the degree of compression, and τ is the induction period behind a rectangular SW. The asterisk denotes a parameter at $r = r_*^C$.

The model shows that (2) can be represented approximately in a simpler form:

$$b = \sigma_0 D_0 \tau_0 \tag{4}$$

where the subscript 0 denotes the parameters behind an SW moving with speed D_0.

Formulas (2) enables one to use the cell measurements to determine the ignition delay and effective activation energy for the conditions corresponding to the detonation temperatures and densities. Comparisons show that the model gives a good fit to a multifront cellular structure. As $D_0\tau_0 = \sigma_0\lambda$ and $b \approx 1.6a$, (4) agrees well with the empirical relation $a \approx 29\lambda$ [90].

The cell size can be derived from the wavelength of the most rapidly growing perturbation, which can be derived from the linear instability treatment for a two-front model [95]. The order of magnitude could be predicted. The best theoretical models involve nonlinear stability analysis, which enables one to determine the main cellular-structure characteristics [96].

A cellular structure has been obtained for a gas detonation from a nonstationary two-dimensional treatment of a weak initial perturbation at a planar front [97-99], which illustrates the scope for simulating detonation by means of the hydrodynamic and chemical-kinetic equations alone (usually simplified). It is possible to trace how weak perturbations grow into transverse waves and generate new waves, as well as to establish the quasiperiodic regular or irregular structure, the formation of unburned gas islands, etc. The calculated structures are very similar to observed ones. The transverse cell size has been calculated [99] for a $2H_2 + O_2 + 60\%Ar$ mixture, which agreed very closely with the measured value ($a = 8.5$ cm for $p_0 = 65$ mm Hg), although the b/a differed appreciably (2.3 instead of the typical 1.6). The value obtained for $b/D_0\tau_0$ in [97] was close to that predicted by (4).

5. INITIATION

A gas detonation is initiated by means of a comparatively low-power source (hot body, weak spark, etc.), with subsequent spontaneous transition to detonation, or else by a source of explosive type (explosive charge, fairly high-power discharge, etc.), which produces an SW that goes over to a self-maintaining detonation (direct initiation). Detonation in a large volume is often excited by a DW emerging from a tube, where the initiation is much easier (detonation emergence). Much attention has recently been given to these phenomena.

Combustion-Detonation Transition. This has been examined in tubes since gas detonation was discovered. The transition occurs because the flame accelerates and impels and compresses the mixture ahead of it, the transition occurring at the critical point, where the conditions for adiabatic self-ignition occur ahead of the front [100-102]. The ignition focus (thermal or chain-thermal explosion) develops with the very rapid formation of a DW in the compressed gas. This wave catches up with the leading shock front and decomposes to give initially an overcompressed DW and then, after weakening, a self-maintaining wave in the unperturbed mixture.

Although the picture as a whole is clear, the main limiting process (predetonation flame acceleration) does not yet have an adequate theoretical description for one to calculate the transition length. The difficulties here are basic and are no less than those for turbulence, which also has a direct bearing on this, since turbulence in the fresh mixture ahead of the flame front is one of the reasons for the acceleration [45]. Flame-surface stretching as a result of a transverse mass-velocity profile in the impelled gas is also important in increasing the combustion rate [2]. Photographs [100, 101] and our observations show that this profile often differs considerably from stationary turbulent flow in a tube: for example, the flame is elongated forward on one side of the channel as a long tongue, which increases the combustion surface considerably. The compressed gas impelled by the less dense combustion products gives rise to a Rayleigh–Taylor instability. The process is complicated by mass transfer through the separating surfaces, which maintains the acceleration as a result of the pressure increase in the products. This effect appears to be decisive in the closing stages, particularly in slow-burning mixtures.

An adiabatic-ignition focus (or foci [100]) in a medium with an induction-time distribution leads to a divergent reaction front; the pressure wave accelerates the ignition and becomes a DW under suitable conditions. The DW dynamics arising from these foci may be examined for a medium containing a temperature or concentration gradient in a one-dimensional treatment by numerical analysis [103, 104].

The distance from the ignition point to the DW point (the transition length) is dependent on the source position and characteristics, as well as on tube roughness and mixture parameters; it can vary widely. The least length (a few times the tube diameter) occurs for fuel–oxygen mixtures in tubes containing large obstacles or roughness such as Shchelkin spirals [45]. Transition lengths of tens of diameters are characteristic of fuel–oxygen mixtures in smooth tubes and fuel–air ones in tubes containing obstacles [2, 50]. At present it is not clear whether there is a finite transition distance for any mixture in a tube whose diameter is greater than the critical value for detonation.

A spherical flame front in a homogeneous unbounded gas can also go over to a detonation. Such a transition has been observed [105] for a $C_3H_8 + 5O_2$ ignited by a wire heated by a current at the center of a spherical volume ($V_0 \approx 1$ m^3, thin rubber shell). However, careful experiments [106] with extremely active mixtures such as $C_2H_2 + O_2$, $C_2H_2 + 2.5O_2$, $C_3H_8 + 5O_2$ and $2H_2 + H_2$ or $CH_4 + 2O_2$ at $p_0 = 2.0$; 4.0; 7.5; 7.7 MPa gave a different result: chambers of diameter 80 and 200 mm with mild ignition at the center from thin electrodes (0.12 mm) did not show the transition outside the zone where the compression wave was reflected form the walls. Obstacles on the path or thicker electrodes (1–2 mm) altered the situation for the acetylene–oxygen mixtures, with the transition occurring before the compression wave reached the wall. In [107], the transition occurred in an ethylene–oxygen mixture at $p_0 \approx 10^5$ Pa after the spherical flame passed through a metal grid.

This indicates that the transition requires marked distortion in the one-dimensional velocity profile ahead of the flame on account of external factors (tube wall, obstacles, etc.). It is insufficient to have small-scale distortions related to turbulence or cellular flame structure [58].

Visible spherical-flame velocities up to 250 m/sec have been attained in fuel–air mixtures after special turbulence-inducing structures [108] or about 100 m/sec in large-scale experiments with free charges [109], but transitions to detonation did not occur.

Detonation Emerging from a Tube into a Large Volume. A planar gas-detonation wave emerging from the end of a tube initiates an undamped detonation in a large volume if the tube diameter exceeds a critical value d_* [110]. This d_* characterizes the detonation capacity. In [18, 71], the mixtures $C_2H_2 + 2.5O_2$, $C_2H_2 + 2.5\ O_2 + 1.25N_2$, $C_2H_2 + 2.5O_2 + 2.5N_2$, $2H_2 + O_2$ and $CH_4 + 2O_2$ were used to demonstrate the relation

$$d_*/a \approx 10 \div 13. \tag{5}$$

Constant d_*/a involves geometrical similarity in the emergence for different mixtures, where the characteristic length scale is the cell size in the stationary detonation wave. However, exact similarity is excluded because the decisive parameters involve several lengths, which correspond in particular to the characteristic reaction-zone sizes, and several independent dimensionless quantities such as γ, Q/c_0^2, and E_a/Q, which characterize the individual mixture features. One expects only approximate similarity if all these paraemters have slight effects apart from one having the dimensions of length (for example, the induction-zone width in the DW), which determines the cell size and the critical emergence diameter. The problem can be elucidated only by experiment.

Measurements have been made on d_* and a for mixtures of the commoner gases over wide concentration ranges, where the maximum tube diameter was 1.83 m [110-117]. Table 1 gives some data for combustible gases mixed with oxygen and air; α is the exponent in the pressure dependence of the critical diameter:

$$d_* = d_{*1}(p_1/p)^{\alpha}. \tag{6}$$

Table 1 shows that (5) is met in most cases, but there are deviations from the average of 13 by almost factors of two in both senses.

Caution is needed in drawing conclusions, where two points need to be remembered. Firstly, d_* and a are not always measured simultaneously, as for example for fuel–oxygen mixtures [112, 113]. Secondly, the cell dimensions are ambiguous in an irregular structure, particularly in methane and fuel–air mixtures. Even the acetylene–oxygen mixtures commonly used in the laboratory give a differing by factors of 1.5-2 with different approaches to cell size determination (average size or dominant size, or else main one a close to maximal). This applies even more so to irregular cells. Our experiments show that fine structures in the imprints are dependent on the soot-layer quality: if the coating is friable, many structure lines are not identified and the cells appear larger. There is thus some uncertainty in the results, which explains the different d_*/a obtained for a given mixture under comparable conditions. The d_* themselves differ little. The most substantial evidence for large deviations from (5) occurs with acetylene–oxygen mixtures having 70-75% Ar added, where the structure is very regular and $d_*/a = 25$ [117].

When a DW is incident normally on a baffle containing a rectangular or circular hole, the critical size for emergence into the volume is the same as that for emergence from a tube with the same cross section [114], so bulk initiation is provided by a narrow region near the front, which is not affected by the elevated pressure arising on baffle reflection.

The critical hole size can be reduced if the center is blocked off to give a ring [117, 118]. The most pronounced effects occur with irregular-cell mixtures for ratios of the inside to outside diameters of the ring $d_2/d_1 = 0.6$-0.7, where the critical emergence pressure is reduced by a factor two for $d_1 = \text{const}$. This is equivalent to approximately the same reduction in d_1 or in the area by an order of magnitude for $p = \text{const}$. More regular-structure mixtures give less effect, as does an annular gap between long coaxial tubes.

Elliptical, triangular, and rectangular holes have been used in [114]; the mixtures were $2H_2 + O_2 + \beta N_2$ and $C_2H_4 + 3(O_2 + \beta N_2)$ at $p_0 = 1$ atm and $1 \leq \beta \leq 3.76$, where it was found that these holes are equivalent to circular ones with the following diameter as regards critical conditions:

$$d_* = 0{,}5\,(d_1 + d_2), \tag{7}$$

where the quantities in parentheses are the diameters of the circumscribed and inscribed circles. Similar measurements with $C_2H_2 + 2.5O_2$ [119] gave (7) replaced by the more accurate relation

TABLE 1. Critical Conditions for Tube Detonation Emergence

Mixture	$10^4 p_0$, Pa	d_*, cm		α	a, cm		d_*/a
$2H_2 + O_2$	1,06	1.9	[110]	—	0,14	[59]	13,6
	1.0	2.0	[112]	1,08	0,15	[59]	13,3
	0,4	5,3	[112]		0,4	[59, 113]	13,3
$CH_4 + 2O_2$	1,06	3.2	[110]	—	0,24÷0,3	[59, 63]	10÷13
	1.0	5.3	[112]	1,05	0,25÷0,3	[59, 63]	16÷21
	0,1	57	[112]		4,4	[113]	13
$C_2H_2 + O_2$	0,1	1,1	[112]	1,07	0,09	[113]	12,2
$C_2H_2 + 2{,}5O_2$	1,06	0.25	[110]	1,07	0.017	[59]	14,5
	1.0	0.2	[115]	0,9	0.018	[59, 115]	11
	0.1	1.6	[115]		0.23	[59, 115]	7
	0.24	0.65	[112]		0,086	[59]	7.6
	0,1	1.7	[112]	1,13	0.13	[113]	13
	0,038	5,3	[112]		0,54	[113]	10
$C_2H_2 + 2{,}5O_2 + 75\%Ar$	0,3	5.2	[117]	1,13	0,23÷0,3	[117]	17÷23
$C_2H_4 + 3O_2$	1.0	0.65	[112]	1,09	—		
" "	0.13	5.3	[112]		0,38	[113]	13,8
$C_2H_6 + 3{,}5O_2$	1.0	1.45	[112]	1,03	—		
$C_3H_8 + 5O_2$	1,0	1,2	[113]	1,07	—		
" "	0.13	10	[112]		0.8	[113]	12,5
$C_4H_{10} + 6{,}5O_2$	1.0	1.3	[113]	—	—		
$29.6\%H_2 + air$	1.0	20	[113]	—	1.5	[113]	13
$17{,}5\%H_2 + air$	1,0	121	[113]	—	12	[113]	10
$56\%H_2 + air$	1.0	121	[113]	—	10	[113]	12
$7{,}75\%C_2H_2 + air$	1.0	12	[113]	—	0,9÷1,0	[63, 113]	12÷13
$12.5\%C_2H_2 + air$	1.0	8	[112]	—	—		
$6{,}54\%C_2H_4 + air$	0.92	45	[113]	—	2.1÷3,3	[113, 116]	13÷21
$4.5\%C_2H_4 + air$	1,0	136	[113]	—	6,7÷8,7	[113, 116]	15÷21
$4\%C_3H_8 + air$	1,0	90	[116]	—	5÷7	[113, 116]	13÷18
$9{,}5\%CH_4 + air$	1,0	—		—	28±3	[116]	—

$$d_* = \sqrt{d_1 d_2}. \tag{8}$$

One can use (7) and (8) for rectangular holes with side ratios H/h < 7. If H/h > 7 (long slot), the emergence becomes two-dimensional and is governed only by the smaller dimension h, whose critical value is

$$h_*/a \approx 3. \tag{9}$$

Two-dimensional DW expansion in a planar channel of small depth H gives [18, 71, 120]

$$h_*/a \approx 10. \tag{10}$$

These measurements were made for H/h ≈ 0.3-0.5 ($C_2H_2 + O_2$, $p_0 \approx 10$ kPa).

Naturally, increasing H in such channels brings h_*/a close to the value corresponding to free emergence from a long slot. When the wall effects governing H vanish [75], it is found for $2H_2 + O_2$ and $C_2H_2 + 2.5O_2 + 70\%$ Ar mixtures that

$$h_*/a = 5 \div 6. \tag{11}$$

We have obtained the same result for $C_2H_2 + 2.5O_2$ if a is measured as the mean for all cells (the imprint is used with the length of the line parallel to the front divided by the number of the oblique lines in one direction intersecting it), and the result coincides with (9) if a is determined as the size fo the predominant large cells almost equal in size and of almost regular rhomb shape. As (9) was derived in [114] for mixtures giving irregular cells, the measurements of a there were ambiguous, and it is evident [116] that h_*/a and d_*/a may vary with the method.

For H/a < 0.3, the detonation propagation conditions in a channel approach the limiting ones, and the wave becomes unstable without change in h, so h_* becomes meaningless. The rapid reduction in H_*/a near H/a ≥ 0.5 is evidently due not only to reduced relative wall loss but also to the transition from two-dimensional cell structures to three-dimensional.

Mechanism research has been performed on DW emergence from a narrow channel to a large volume [71, 120-122]; Fig. 4 shows the main points. The wave flanks weaken immediately

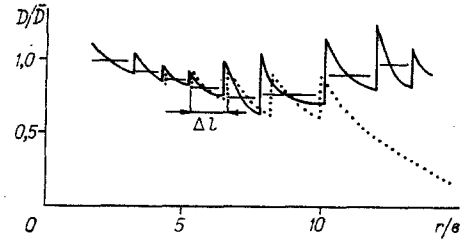

Fig. 6. DW velocity behavior on initiation; the points represent damping, while the lines are for the transcritical state.

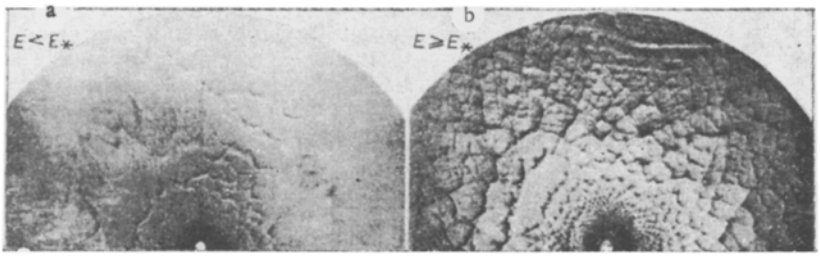

Fig. 7. Impressions from detonation initiation.

beyond the end, with approximately self-similar expansion. Ignition behind them ceases, and the transverse waves emerging from the central zone do not collide and decay rapidly. If the channel dimensions are subcritical, the central region, which has a cellular structure, contracts to zero and the detonation terminates. With supercritical ones, this contraction is replaced by expansion. There are definitely two mechanisms for this. The first is that a self-maintaining transverse DW is formed, which propagates in the shock-compressed gas along the flank of the diffracting front away from the center. That wave initiates an overcompressed but gradually attenuating oblique detonation front in the adjacent unperturbed mixture. As the latter decays, the process may repeat. The second mechanism is that new transverse waves are generated at the flanks, which move towards the center, and which may arise from self-ignition foci and interactions with these or with other inhomogeneities in the damped colliding waves.

With critical dimensions, the detonation region in the initial front contracts almost to zero, but then the detonation structure recovers, usually by the first mechanism on collision in the shock-compressed layer (above the vertex of the vanishing detonation cone) by collision between two already attenuated new transverse waves generated at the opposite flanks, or else of such a wave with one of the later transverse waves in the initial family.

Several theoretical methods of estimating d_*/a or h_*/a exist, which give results close to experiment. All are based on the ignition termination condition behind a convex shock front in some form. For example, in [71, 123], the condition was for critical temperature drop along the radius, while in [121, 122] it was the same along the curved shock front, and in [124, 125] it was the condition for critical curvature in a quasistationary one-dimensional detonation wave. In the last case, the result for the critical radius of curvature was $r_{cr} \approx (3\text{-}4)b$ for a cylindrical front or $r_{cr} \approx (6\text{-}8)b$ for a spherical one. If it is assumed that the critical-curvature state corresponds to a region behind the collision point for the transverse waves reflected from the channel edges ($r_{cr} \approx d_*$), the results $d_*/a \approx 1.6r_{cr}/b$ agree satisfactorily with the measurements.

Direct Initiation. The methods here are with condensed explosives, explosion of another gas mixture, electrical wire explosion, high-voltage sparks, and laser sparks.

The conditions are characterized by the critical (minimal) energy $E_{*\nu}$ required to produce an SW going over to a self-maintaining detonation; $\nu = 1, 2, 3$ denotes planar, cylindrical, and spherical waves correspondingly. In general, $E_{*\nu}$ is dependent on the energy distributions in time and space, which can be characterized from the effective time Δt and size ΔR. The latter in particular is indicated as having a marked effect for detonation emergence

from circular and annular holes. The characteristic length and time scales for a front, which can be compared with ΔR and Δt, are b or a and $t_c = b/D$.

Careful time-factor measurements were made in [126] for cylindrical initiation by a line spark in a $C_2H_2 + 2.5O_2$ mixture ($p_0 = 13$ kPa). A current-interruption circuit was used to show that a periodic current produces an effect only from the first quarter period. The point condition ($\Delta R \leq b$) and the instantaneous one ($\Delta t \leq t_c$) are certainly met with critical-mass explosive charges.

With $\Delta R < b$ and $\Delta t < t_c$, the initiation is similar in general features as regards symmetry for all mixtures; this may be considered from the variable wave speed D(r) (Fig. 6) and the cellular structure (Fig. 7) recorded for acetylene–oxygen with cylindrical discharge initiation in a flat gap under transcritical conditions [80, 115, 127]. The initial stage is analogous to that of a strong explosion in a nonreacting gas, with the wave parameters decreasing. Before the speed has fallen to D_0, small cells appear at the front and then larger ones. At the same time, the velocity fall becomes slower and local pulsations arise in connection with the cell structure. For $E_2 \geq E_{*2}$, the mean velocity has a minimum at a certain radius, while the cell size is maximal, after which the two tend gradually to their stationary mean values. When $E_2 \gg E_{*2}$, the turning points in D and b become inappreciable.

If $E_2 = E_{*2}$, the wave excited by an explosion shows a critical stage in the region $r_{cr} = (5\text{-}8)b$: the combustion zone is separated from the SW [35, 102], while the cellular structure vanishes and is replaced by a quasi-one-dimensional one; the adiabatic ignition temporarily ceases. Then the leading edge increases in speed to $D > D_0$, and after a few oscillations reaches the state corresponding to a stationary DW; sometimes, there are two or three large oscillations with deep velocity dips. Schlieren pictures show that the front begins to accelerate usually with increased local convexity, which then extends to the entire front, and the shock-compressed gas shows a transverse DW [35]. This can be seen on impressions analogous to those of Fig. 7. Cases also occur where a large part of the front accelerates almost simultaneously.

Detonation reinitiation after front decay in the critical stage does not differ essentially from that observed in the final stage of combustion-detonation transition or in DW recovery on exit to a large volume from a critical channel: the detonation begins in the gas compressed by the SW because an adiabatic ignition focus develops, which is usually stimulated by perturbation waves. If $E_2 < E_{*2}$, the ignition halts at a point $r < r_{cr}$ where $D < D_0$, and the shock wave is detached from the flame and gradually decays (dotted curve in Fig. 6).

Similar speed variations occur in spherical initiation with various mixtures, including large-scale experiments, where radio interferometry was used to record the ignition zone [128-130]. In the spherical case ($\nu = 3$), the wave passes through a critical stage at a distance $r_{cr} \approx (8\text{-}12)b$ from the center. In the planar case ($\nu = 1$), there is indirect evidence [131] that $r_{cr} \approx (2\text{-}4)b$ in the case of fuel–air mixtures initiated by sheet explosive charges. The measurements for all cases together satisfy

$$r_{cr} \simeq (2 \div 4)\nu \cdot b. \qquad (12)$$

Near-stationary detonation parameters occur for $r \approx 2r_{cr}$ [115, 127]. The minimum shock-wave speed D_{min} for critical initiation conditions shows no obvious dependence on ν or on mixture composition and is $(0.5\text{-}0.6)D_0$ [127-132]. This very low D_{min} does not determine however the critical ignition delays in the induction zone behind a nonstationary wave: when the minimum velocity is attained, the shock front is strengthened by a compression wave or DW formed in the induction zone by collisions between old attenuated transverse waves or by self-ignition in the parts of the gas intersected by the front much earlier.

When the initiation is by a wave with approximately constant parameters in a shock tube [132] or is by an electric spark [126], the SW parameters in the region $\Delta t \gtrsim 2t_c$ do not have an initial falling part, so there is no preliminary adiabatic ignition, transverse-wave generation, or ignition termination, although the other processes are analogous to the above. The electrode shape affects spark initiation; conditions have been defined under which cylindrical initiation is replaced by spherical; and excitation by wire explosion or laser spark shows no essential difference from electrical spark initiation [102]. With a laser spark, a solid target (tip of a metal needle) was used to reduce the breakdown

TABLE 2. Stoichiometric-Mixture Critical Initiation Energies

Mixture	p_0, 10^5 Pa	ν	Initiator	$E_{*\nu}$, J·m$^{\nu-3}$	$\frac{(E_{*\nu}/p_0)^{1/\nu}}{d_*}$	Ref.
$C_2H_2 + 2{,}5O_2$	0,024	2	Wire explosion	270	3,8	[127]
	0,052	2	"	100	3,7	[127]
	0,066	2	Spark	22	2,1	[133]
	0,13	2	»	11,5	2,3	[133]
	0,27	2	»	6,3	2,7	[133]
	0,4	2	»	4,5	2,9	[133]
$2H_2 + O_2$	0,5	2	Spark	300	1,8	[102]
	0,5	2	Wire explosion	460	2,3	[127]
C_2H_2 + air	1	2	Solid explosive	$2{,}3\cdot10^4$	4,0	[115]
	1	3	»	$4{,}6\cdot10^3$	3,0	[130]
H_2 + air	1	3	Solid explosive	$4{,}6\cdot10^3$	1,8	[113]
	1	3	»	$6{,}3\cdot10^3$	2,0	[130]
C_2H_4 + air	1	3	Solid explosive	$4{,}4\cdot10^4$	1,7	[130]
C_2H_6 + air	1	3	»	$1{,}6\cdot10^5$		[130]
C_3H_8 + air	1	3	»	$3{,}4\cdot10^5$	1,7	[130]
C_4H_{10} + air	1	3	»	$3{,}4\cdot10^5$		[130]
C_4H_{10} + air	1	3	»	$4{,}2\cdot10^5$		[130]
CH_4 + air	1	1	$2H_2 + O_2$	10^6*	2,5†	[132]
	1	1	Solid explosive	$\sim10^6$		[131]
	1	3	»	$9\cdot10^7$*	2,4†	[130]

*β extrapolation for the following mixtures: $CH_4 + 2(O_2 + \beta N_2)$ and $CH_4 + \beta C_2H_6$ + air.
†For $d_* = 13a = 4$ m.

threshold in an acetylene–oxygen mixture. The critical pulse energy was then several times higher than in electric spark initiation [133]. This is ascribed to some of the pulse energy being dissipated in the target and by reflection from the breakdown region. There is also a terminal decaying part to a laser pulse, as usually also for an electrical one. It is not always clear whether this contributes to the effects if the pulse length is short. It has been asserted [126] that the initiation is provided only by the rising part, but this is of restricted application, since it implies in particular that a square pulse of any energy or length cannot initiate the detonation if the energy in the rising part is less than E_*.

Table 2 gives the measured $E_{*\nu}$ for common stoichiometric mixtures. The initiation energy for the solid explosives has been taken as the product of the mass by the standard heat of explosion, i.e., it is assumed that the detonation is complete. With charges of mass about 1 g or less, there is no certainty of this, so the E_{*3} for the acetylene–air mixture is probably overestimated. A more objective method of determining the energy for small explosive charges is based on comparing the r–t diagram for the SW in an inert gas with theoretical diagrams for point explosions [127, 132]. The methane–air mixture shows the highest detonation resistance, but no direct measurements have been made on E_{*3}, in spite of the great practical interest, because of the excessive scale required (it is necessary to record the spherical front up to a radius of ∿10 m). The initiation energy is dependent on the oxidant–fuel ratio, and this is U-shaped, as for the rleation between a and d_*, with a minimum at the stoichiometric composition or slightly on the enriched side [34].

Stoichiometric and lean mixtures give [90]

$$E_{*3} = A\lambda^3, \tag{13}$$

where A ≈ const. This relation resembles (5)-(12) in reflecting the approximate similarity. For rich mixtures such as C_2H_4 in air, there are substantial deviations from (13), i.e., similarity deviations [34]. Formula (13) is suitable for estimating initiation energies for a mixture when data are available on λ. The form corresponds to the conclusion of [110]. A can be determined without resort to experiment from several model approaches, some of which are considered in [134].

The one-dimensional closed model of [80, 135] reflects the main features correctly; this assumes that the initiated DW propagates via two processes: 1) instantaneous shock-compressed gas combustion and corresponding increase in the front speed at the end of the induction period behind the rear layer edge, and 2) SW motion without ignition at a falling rate, where the corrected interpolation formulas of [94] can be used. The critical explosion energy is taken as the minimum value for which ignition occurs in a finite time after termination at any distance from the center, or in fact at the most hazardous critical value defined in the model. The final general expressions for the critical parameters are

$$E_{*\nu} \simeq 0{,}2\left(\frac{E_a}{RT}\right)^{\nu} \rho_0 D_0^3 b^{\nu}, \quad r_{\nu}^{*} \simeq 0{,}2\nu \frac{E_a}{RT} b, \tag{14}$$

where $r_{*\nu}$ is the critical termination point, which is about three times closer to the center than the minimum-velocity one.

The critical energy is always related to a certain wave radius, beyond which the wave is capable of self-maintaining propagation. In [136, 137], the relationship was derived from the condition $D(r_*) = D_0$ for a strong point explosion in a reacting gas, while r_* was estimated from a condition for cellular-structure reproduction in an expanding front. Then

$$E_{*3} = \left(0{,}31\frac{\rho u^2}{2} + 0{,}59\frac{p}{\gamma - 1} - \rho_0 Q - \frac{p_0}{\gamma_0 - 1}\right)\cdot\frac{4}{3}\pi r_*^3, \tag{15}$$

$$r_* \simeq \frac{40}{\gamma - 1} D_0 \tau_0 \sigma_0,$$

where the unsubscripted quantities relate to the Chapman–Jouguet state behind the stationary wave.

In [125], use was made of the relation between $E_{*\nu}$ and the wave radius r_{min} at the minimum velocity, which was fitted to numerical experiments on gas-droplet systems, with the result taken as universal, while r_{min} was equated to the minimum radius of curvature for a stationary two-front wave. This gave formulas for E_* in the cylindrical and spherical cases:

$$E_{*\nu} = a_\nu p_0 r_0^{\nu} \approx a_\nu p_0 \left(\frac{8}{\nu} r_{\min}\right)^{\nu},$$

$$r_{\min} \simeq 4(\nu - 1)\gamma^2(\sigma_0 + 1/\sigma_0 - 2)\frac{E_a}{RT}\lambda, \tag{16}$$

where a_ν is a factor of the order of one, dependent on γ and ν, derived from point-explosion theory [138]. The factor $\nu - 1$ in the latter expression does not allow one to calculate E_{*1}, but incorporating nonstationary effects should lead to $\nu - 1$ being replaced by ν [139] in accordance with (12) and (14). Then (16) agrees with the following apart from the factor a_ν:

$$r_0 \equiv (E_{*\nu}/p_0)^{1/\nu} \simeq \text{const}, \tag{17}$$

which was derived in [102] by comparing measurements for different ν. If the initiation energy is known for one symmetry case, one can estimate $E_{*\nu}$ for other ν from (17).

The following expression has been derived [139] from simulation and extrapolation to zero droplet size:

$$E_{*\nu} \simeq a_\nu p_0 \left(\frac{150}{\sigma_0^{\xi}} b\right)^{\nu}, \quad \xi = 1 \div 2. \tag{18}$$

From (5), this can be put in the simplest form:

$$E_{*\nu} \simeq p_0 (B d_*)^{\nu}, \quad B = \frac{20}{\sigma_0^{\xi}}, \tag{19}$$

which agrees well with experiment (Table 2).

The model of [140, 141] is based on the cellular structure directly, and it implies

$$E_{*1} \simeq n \cdot 0{,}4\rho_0 D_0^2 b, \quad E_{*2} = 2{,}3\rho_0 D_0^2 b^2, \quad E_{*3} \simeq 9\rho_0 D_0^2 b^3. \tag{20}$$

Here allowance is made for the energy in the transverse-wave collision region of (3), which initiates leading-front motion within a cell, as well as the critical number of cells at the surface, which is determined from experiments on detonation emergence from a slot or

tube. Here n = 1 or 2 if there are transverse waves in one or two mutually perpendicular planes correspondingly. If the initiation source is not a point and not instantaneous, and $\Delta R + \bar{D}\Delta t > b$, it has been suggested that $E_{*\nu}$ should be increased by the factor $(\Delta R/b + \bar{D}\Delta t/b)^{\nu-1}$, which incorporates the initiating-wave surface growth. The possible variations in d_*/a with the mixture and pressure have been incorporated [115] on modifying this model:

$$E_{*\nu} \simeq 0{,}4\rho_0 D_0^2 (d_*/a)^{\nu-1} b^\nu, \quad \nu = 2; 3. \tag{21}$$

In [34, 113], the initiation criterion for a strong point explosion was that the area of a spherical shock wave front at the instant when its velocity falls to D_0 is equal to the area of a planar DW front in a tube of diameter d_*. Then

$$E_{*3} = 4\pi I \rho_0 D_0^2 (d_*/4)^3 \simeq 50\rho_0 D_0^2 b^3 \tag{22}$$

(the factor 50 is obtained if $d_* = 13a = 8.5b$). It has been shown [134] that (21) and (22) give a description better than the other models considered there, which are not quoted in this review.

The model of [140, 141] is the only one in which $E_{*\nu} \sim d_*^{\nu-1}$, i.e., is proportional to the critical-radius front area. At present, appropriate measurements are inadequate for identical mixtures with different ν for one to conclude whether $E_{*\nu} \sim d_*^\nu$ or $E_{*\nu} \sim d_*^{\nu-1}$ is better. The various models and formulas given here give initiation energies of the same order of magnitude.

Practical $E_{*\nu}$ estimates can be derived from (19) with $\xi = 1$ and $d_* = 13a \approx 8\sigma_0^2\lambda = 8\sigma_0 D_0 \tau_0$, as well as from (21) and (22).

Detonation initiation simulation in a one-dimensional formulation ($2H_2 + O_2$) [142] gave the main qualitative characteristics correctly; however, the initial conditions for a self-similar point explosion resulted in very much overestimated initiation energies, primarily because the one-dimensional model has limitations related to detonation-front instability. The initial conditions for a finite region ($H_2 + Cl_2$) gave initiation energies of the measured order [143].

6. CONCLUSIONS

Although an actual detonation-front structure in a gas is always in more than one dimension (cellular or spin), the one-dimensional theory gives good predictions not only for the speed but also for certain internal characteristics, in particular the peak in the mean pressure acting at the wall in the forward and reflected waves. There are some wave parameters where the predictions from the theory deviate from experiment, although some of them such as ψ tend to approach the theoretical values as d/a increases, while other differ substantially from the predictions but their scales are correlated with the cell-structure size, such as parameter profiles, effective front thickness, and distance to the Chapman–Jouguet surface.

There are macrokinetic effects from the inhomogeneous structure; these are of two types. On the one hand, the effective induction time is reduced, with the reaction starting directly at the front, while on the other, the inhomogeneities lengthen the energy-deposition zone, which is found to be larger by an order of magnitude than that envisaged in the one-dimensional theory. Consequently, the parameter profiles deviate from the almost rectangular form corresponding to the one-dimenisonal theory and becomes triangular, even for high activation energies.

Extremely detailed experiments have been performed on major inhomogeneous-structure elements in stationary DW, as well as on certain transient phenomena such as emergence from a tube into a large volume or direct initiation. The theoretical and numerical descriptions sometimes fit the observations well, but sometimes they lead us to desire better. Semiempirical models appear to be the most effective in some cases, such as for the initiation energy.

Current topics are: stationary and nonstationary flame propagation in the speed range 10^1-10^3 m/sec, which is a range intermediate for classical combustion and detonation, particularly in channels, encumbered spaces, and in free volumes; spin and cellular DW stability in long tubes; detonation limits, in particular for spin and galloping modes; the effects of scale factors on DW initiation and propagation in large explosions; and the physical and chemical processes in DW interaction with suspended particles, obstacles, and walls, including explosion safety and engineering gas-detonation applications.

LITERATURE CITED

1. B. V. Voitsekhovskii, V. V. Mitrofanov, and M. E. Topchiyan, Fiz. Goreniya Vzryva, 5, No. 3 (1969).
2. Ya. B. Zel'dovich and A. S. Kompaneets, Detonation Theory [in Russian], Gostekhizdat, Moscow (1955).
3. S. M. Kogarko and Ya. B. Zel'dovich, Dokl. Akad. Nauk SSSR, 63, 526 (1948).
4. G. B. Kistiakowsky and P. H. Kidd, J. Chem. Phys., 25, No. 5, (1956).
5. R. E. Duff and T. Knight, ibid., 25, No. 6.
6. D. R. White, Phys. Fluids, 4, No. 4 (1961).
7. D. H. Edwards, G. T. Williams, and J. C. Breeze, J. Fluid Mech., 6, No. 4 (1959).
8. R. I. Soloukhin, Prib. Tekh. Eksp., No. 3 (1961).
9. V. V. Mitrofanov and V. A. Subbotin, Continuous-Medium Dynamics [in Russian], Issue 9, Novosibirsk (1971).
10. A. V. Vasil'ev, T. P. Gavrilenko, and M. E. Topchiyan, Fiz. Goreniya Vzryva, 9, No. 5 (1973).
11. A. N. Dremin, S. D. Savrov, V. S. Trofimov, et al., Detonation Waves in Condensed Media [in Russian], Nauka, Moscow (1970).
12. A. V. Vasil'ev, Ph. D. Thesis, IG SO AN SSSR (1974).
13. A. V. Vasil'ev, T. P. Gavrilenko, and M. P. Topchian, Astron. Acta, 17, No. 4-5 (1972).
14. A. V. Vasil'ev, T. P. Gavrilenko, V. V. Mitrofanov, et al., Fiz. Goreniya Vzryva, 8, No. 1 (1972).
15. T. V. Bazhenova, L. G. Gvozdeva, et al., Gas Shock Waves [in Russian], Nauka, Moscow (1968).
16. A. V. Vasil'ev, T. P. Gavrilenko, and M. E. Topchiyan, Fiz. Goreniya Vzryva, 9, No. 2 (1973).
17. D. H. White, Phys. Fluids, 4, No. 4 (1961).
18. B. V. Voitsekhovskii, V. V. Mitrofanov, and M. E. Topchiyan, Detonation-Front Structures in Gases [in Russian], Izd. SO AN SSSR, Novosibirsk (1963).
19. S. S. Rybanin, Fiz. Goreniya Vzryva, 2, No. 1 (1966).
20. M. E. Topchiyan, D. Sc. Thesis, IG SO AN SSSR (1974).
21. Yu. A. Nikolaev and M. E. Topchiyan, in: Combustion and Explosion [in Russian], Nauka, Moscow (1977), p. 461.
22. J. Eisen, R. Gross, and T. Rivlin, Vop. Raket. Tekh., No. 1 (1961).
23. Yu. A. Nikolaev and M. E. Topchiyan, Fiz. Goreniya Vzryva, 13, No. 3 (1977).
24. V. M. Vasil'ev, A. I. Vol'pert, et al., Fiz. Goreniya Vzryva, 1, No. 3 (1960).
25. Yu. A. Nikolaev, M. E. Topchiyan, and V. Yu. Ul'yanitskii, Fiz. Goreniya Vzryva, 14, No. 6 (1978).
26. N. S. Astapov, Yu. A. Nikolaev, and V. Yu. Ul'yanitskii, Fiz. Goreniya Vzryva, 20, No. 1 (1984).
27. Yu. A. Nikolaev, Fiz. Goreniya Vzryva, 14, No. 4 (1978).
28. R. A. Strehlow, R. E. Maurer, and S. Rajan, AIAA J., 7, No. 2 (1969).
29. Yu. A. Nikolaev, Fiz. Goreniya Vzryva, 15, No. 3 (1979).
30. D. H. Edwards, T. G. Jones, and B. Price, J. Fluid Mech., 17, No. 1 (1963).
31. A. A. Vasil'ev, Fiz. Goreniya Vzryva, 12, No. 3 (1975).
32. V. Rozing and Yu. B. Khariton, Dokl. Akad. Nauk SSSR, 26, 360 (1939).
33. V. I. Manzhalei and V. V. Mitrofanov, Fiz. Goreniya Vzryva, 9, No. 5 (1973).
34. J. H. Lee, Ann. Rev. Fluid Mech., 16, 311 (1984).
35. J. H. Lee, R. I. Soloukhin, and A. K. Oppenheim, Astron. Acta, 14, 565 (1969).
36. A. A. Vasil'ev, Fiz. Goreniya Vzryva, 23, No. 3 (1987).
37. P. Wolanskii, C. M. Kauffman, et al., 18th Internat. Symposium on Combustion, Canada (1980).
38. N. Manson, C. Brochet, et al., 9th Internat. Symposium on Combustion, USA (1963).
39. V. Yu. Ul'yanitskii, Fiz. Goreniya Vzryva, 17, No. 1 (1981).
40. A. A. Vasil'ev, Fiz. Goreniya Vzryva, 18, No. 3 (1982).
41. A. A. Vasil'ev, and V. A. Subbotin, Continuous-Medium Dynamics [in Russian], No. 62, Novosibirsk (1983).
42. A. A. Vasil'ev and D. V. Zak, Fiz. Goreniya Vzryva, 22, No. 4 (1986).
43. M. F. Ivanov, V. E. Fortov, and A. A. Borisov, Fiz. Goreniya Vzryva, 17, No. 3 (1981).
44. M. F. Ivanov, V. N. Shebeko, and A. Ya. Korol'chenko, Fiz. Goreniya Vzryva, 19, No. 2 (1984).

45. K. I. Shchelkin, Fast Combustion and Detonation in Gases [in Russian], Oborongiz, Moscow (1949).
46. V. S. Babkin and L. S. Kozachenko, Zh. Prikl. Mekh. Tekh. Fiz., No. 3 (1969).
47. Ya. B. Zel'dovich, A. A. Borisov, et al., Dokl. Akad. Nauk SSSR, 279, No. 6 (1984).
48. G. M. Mamontov, V. V. Mitrofanov, and V. A. Subbotin, in: Detonation [in Russian], Chernogolovka (1980), p. 106.
49. V. A. Subbotin and A. Ya. Kuznetsova, Continuous-Medium Dynamics [in Russian], No. 68, Novosibirsk (1984).
50. J. H. Lee, R. Knystautas, and A. Freiman, Combust. Flame, 56, 227 (1984).
51. J. H. Lee, Progr. Astron. Aeron., 106, No. 3 (1985).
52. Ya. B. Zel'dovich and A. A. Borisov, Khim. Fiz., 4, No. 2 (1985).
53. A. A. Vasil'ev, Fiz. Goreniya Vzryva, 18, No. 2 (1982).
54. C. W. Kaufman, Y. Chuanjun, and J. A. Nicholls, 19th Internat. Symposium on Combustion, Israel (1982).
55. G. A. Lyamin and A. V. Pinaev, Dokl. Akad. Nauk SSSR, 283, No. 6 (1985).
56. G. A. Lyamin and A. V. Pinaev, Fiz. Goreniya Vzryva, 22, No. 5 (1986).
57. G. A. Lyamin, V. V. Mitrofanov, et al., in: Detonation and Shock Waves [in Russian], Chernogolovka (1986), p. 52.
58. Ya. K. Troshin and K. I. Shchelkin, Combustion Gas Dynamics [in Russian], Izd. Akad. Nauk SSSR, Moscow (1963).
59. V. I. Manzhalei, V. V. Mitrofanov, and V. A. Subbotin, Fiz. Goreniya Vzryva, 10, No. 1 (1974).
60. V. I. Manzhalei and V. V. Mitrofanov, Fiz. Goreniya Vzryva, 9, No. 5 (1973).
61. R. A. Strehlow and C. D. Engel, AIAA J., 7, No. 3 (1969).
62. J. C. Libouton, M. Dormal, and P. J. Van Tiggelen, 15th Internat. Symposium on Combustion, Japan (1974).
63. D. C. Bull, J. E. Elsworth, et al., Combust. Flame, 45, No. 7, (1982).
64. A. A. Borisov and S. A. Loban', Fiz. Goreniya Vzryva, 13, No. 5 (1977).
65. A. A. Vasil'ev, M. E. Topchiyan, and V. Yu. Ul'yanitskii, Fiz. Goreniya Vzryva, 15, No. 6 (1979).
66. V. I. Manzhalei, V. A. Subbotin, and V. A. Shcherbakov, in: Detonation [in Russian], Chernogolovka (1977), p. 45.
67. M. Dormal, J.-C. Libouton, and P. J. Van Tiggelen, Acta Astron., 6, 875 (1979).
68. R. A. Strehlow, A. A. Adamzyk, and R. J. Stiles, Astron. Acta, 17, 509 (1972).
69. S. M. Kogarko, Izv. Akad. Nauk SSSR, OKhN, No. 4 (1956).
70. R. A. Strehlow and R. J. Salm, Acta Astron., 3, 983 (1976).
71. V. V. Mitrofanov and R. I. Soloukhin, Dokl. Akad. Nauk SSSR, 159, No. 5 (1964).
72. A. A. Vasil'ev, Fiz. Goreniya Vzryva, 21, No. 2 (1985).
73. T. V. Bazhenova, L. G. Gvozdeva, et al., Nonstationary Shock and Detonation Wave Interactions in Gases [in Russian], Nauka, Moscow (1986).
74. S. A. Gubin, S. M. Kogarko, and V. N. Mikhalkin, Fiz. Goreniya Vzryva, 18, No. 5 (1982).
75. G. O. Thomas and D. H. Edwards, Progr. Astron. Aeron., 106, 144 (1985).
76. A. A. Vasil'ev and Yu. A. Nikolaev, in: Combustion and Explosion Chemical Physics: Detonation [in Russian], Chernogolovka (1977), p. 49.
77. T. P. Gavrilenko and E. M. Prokhorov, Fiz. Goreniya Vzryva, 17, No. 6 (1981).
78. V. I. Manzhalei and V. A. Subbotin, Fiz. Goreniya Vzryva, 12, No. 6 (1976).
79. V. I. Manzhalei, Fiz. Goreniya Vzryva, 15, No. 4 (1979).
80. V. Yu. Ul'yanitskii, Fiz. Goreniya Vzryva, 17, No. 2 (1981).
81. J. J. Erpenbek, Phys. Fluids, 7, No. 5 (1964).
82. V. I. Manzhalei, Ph. D. Thesis, IGiL SO AN SSSR (1981).
83. E. A. Lundstrom and A. K. Oppenheim, Proc. R. Soc., A310, 463 (1969).
84. D. H. Edwards, G. Hooper, et al., Astron. Acca, 15, No. 5/6 (1970).
85. R. A. Strehlow and A. J. Crooker, Acta Astron., 1, No. 3/4 (1974).
86. V. A. Subbotin, Fiz. Goreniya Vzryva, 12, No. 3 (1976).
87. V. V. Mitrofanov and V. A. Subbotin, in: Combustion and Explosion [in Russian], Nauka, Moscow (1977), p. 447.
88. V. A. Subbotin, Fiz. Goreniya Vzryva, 11, No. 3 (1975).
89. V. A. Subbotin, Fiz. Goreniya Vzryva, 11, No. 1 (1975).
90. C. Westbrook and P. A. Urt'ev, Fiz. Goreniya Vzryva, 19, No. 6 (1983).
91. R. A. Strehlow and F. D. Fernandes, Combust. Flame, 9, 109 (1965).

92. H. O. Barthel, Phys. Fluids, 17, 1547 (1974).
93. A. A. Vasil'ev and Yu. A. Nikolaev, Fiz. Goreniya Vzryva, 12, No. 5 (1976).
94. A. A. Vasil'ev, Yu. A. Nikolaev, and V. Yu. Ul'yanitskii, Fiz. Goreniya Vzryva, 13, No. 3 (1977).
95. V. L. Maloryan, A Method of Calculating Pulsating-Structure Elements in Gas Detonation [in Russian], Dep. Ukr. NIINTI No. 3479-Uk85 Dep.
96. V. A. Danilenko and V. M. Kudinov, Abstracts for the All-Union Conference on the Lavrent'ev Lectures [in Russian], IGiL SO AN SSSR, Novosibirsk (1982), p. 67.
97. S. Taki and T. Fujiwara, AIAA J., 16, 93 (1978).
98. V. V. Markov, Dokl. Akad. Nauk SSSR, 252, No. 2 (1981).
99. K. Kailasanath, E. S. Oran, et al., Combust. Flame, 61, 199 (1985).
100. R. I. Soloukhin, Shock Waves and Detonation in Gases [in Russian], Fizmatgiz, Moscow (1963).
101. P. A. Urtiew and A. K. Oppenheim, Proc. R. Soc., A295, No. 13 (1966).
102. J. H. Lee, Ann. Rev. Phys. Chem., 28, 75 (1977).
103. Ya. B. Zel'dovich, V. B. Librovich, G. M. Makhviladze, et al., Zh. Prikl. Mekh. Tekh. Fiz., No. 2 (1970).
104. B. E. Gel'fand, S. M. Frolov, A. N. Polenov, et al., Khim. Fiz., 5, No. 9 (1986).
105. S. M. Kogarko, V. V. Adushkin, and A. G. Lyamin, NTPGV, 1, No. 2 (1965).
106. A. G. Podgrebenkov, B. E. Gel'fand, et al., Dokl. Akad. Nauk SSSR, 184, No. 4 (1969).
107. G. Wagner, K. Dorge, and D. Pangritz, Acta Astron., 3, No. 6 (1976).
108. V. A. Gorev and S. N. Miroshnikov, Khim. Fiz., 1, No. 6 (1982).
109. V. I. Makeev, Yu. A. Gostintsev, et al., Fiz. Goreniya Vzryva, 20, No. 5 (1984).
110. Ya. B. Zel'dovich, S. M. Kogarko, and N. N. Simonov, Zh. Tekh. Fiz., 26, No. 8 (1956).
111. D. H. Edwards, M. A. Nettleton, and G. O. Thomas, J. Fluid Mech., 95, 79 (1979).
112. H. Matsui and J. H. Lee, 17th Internat. Symp. on Combustion, England (1978).
113. J. H. Lee, R. Knystautas, and G. M. Guirao, in: Fuel–Air Explosions, Toronto (1982).
114. Y. K. Liu, J. H. Lee, and R. K. Knystautas, Combust. Flame, 56, 215 (1984).
115. A. A. Vasil'ev and V. V. Grigor'ev, Fiz. Goreniya Vzryva, 16, No. 9 (1980).
116. I. O. Moen, J. W. Wunk, S. A. Ward, et al., Progr. Astron. Aeron., 94, 55 (1984).
117. I. O. Moen, G. O. Sulmistras, G. O. Thomas, et al., Progr. Astron. Aeron., 106 (1986).
118. A. A. Vasil'ev, in: Fundamental Problems in Shock-Wave Physics [in Russian], Chernogolovka (1987).
119. A. A. Vasil'ev, Continuous-Medium Dynamics [in Russian], Issue 78, Novosibirsk (1987).
120. B. V. Voitsekhovskii, in: Scientific Council on Economic Use of Explosions [in Russian], Issue 13, Izd. Sib. Otd. Akad. Nauk SSSR, Novosibirsk (1960).
121. D. H. Edwards and G. O. Thomas, Progr. Astron. Aeron., 75, 341 (1981).
122. V. V. Mitrofanov and V. A. Subbotin, 8th ICOGERS, Minsk (1981): Book of Abstracts.
123. R. I. Soloukhin, 12th Internat. Symp. on Combustion, France (1968).
124. V. V. Mitrofanov, Detonation Theory [in Russian], NGU, Novosibirsk (1982).
125. V. V. Mitrofanov, Fiz. Goreniya Vzryva, 19, No. 4 (1983).
126. R. Knystautas and J. H. Lee, Combust. Flame, 27, 221 (1976).
127. A. A. Vasil'ev, Fiz. Goreniya Vzryva, 19, No. 1 (1983).
128. D. H. Edwards, G. Hooper, and J. M. Morgan, Acta Astron., 3, 117 (1976).
129. D. Desbordes, N. Manson, and J. Brossard, Progr. Astron. Aeron., 75 (1981).
130. D. C. Bull, in: Fuel–Air Explosions, Toronto (1982).
131. W. B. Benedick, Combust. Flame, 35, 87 (1979).
132. S. Ohyagi, T. Yoshihashi, and Y. Harigaya, Progr. Astron. Aeron., 94, No 3 (1984).
133. J. H. Lee and H. Matsui, Combust. Flame, 28, 61 (1977).
134. M. B. Benedick, C. M. Guirao, et al., Progr. Astron. Aeron., 106, 181 (1985).
135. V. Yu. Ul'yanitskii, Fiz. Goreniya Vzryva, 16, No. 3 and 16, No. 4 (1980).
136. K. Ya. Troshin, Dokl. Akad. Nauk SSSR, 247, No. 4 (1979).
137. A. A. Borisov, V. M. Zamanskii, et al., Khim. Fiz., 5, No. 12 (1986).
138. L. I. Sedov, Similarity and Dimensional Methods in Mechanics [in Russian], Nauka, Moscow (1972).
139. S. A. Zhdan and V. V. Mitrofanov, Fiz. Goreniya Vzryva, 21, No. 6 (1985).
140. A. A. Vasil'ev, Fiz. Goreniya Vzryva, 14, No. 3 (1978).
141. A. A. Vasil'ev, Yu. A. Nikolaev, and V. Yu. Ul'yanitskii, Fiz. Goreniya Vzryva, 15, No. 6 (1979).
142. V. A. Levin and V. V. Markov, Fiz. Goreniya Vzryva, 11, No. 4 (1975).
143. V. A. Levin, V. V. Markov, and S. F. Osinkin, Khim. Fiz., 3, 4 (1984).